Atmos. Chem. Phys., 16, 10651–10669, 2016
www.atmos-chem-phys.net/16/10651/2016/
doi:10.5194/acp-16-10651-2016

Atmospheric Chemistry and Physics Open Access EGU

Evaluating secondary inorganic aerosols in three dimensions

Keren Mezuman[1,2], **Susanne E. Bauer**[3,2], **and Kostas Tsigaridis**[3,2]

[1]Earth and Environmental Sciences, Columbia University, New York, NY, USA
[2]NASA Goddard Institute for Space Studies, New York, NY, USA
[3]Center for Climate Systems Research, Columbia University, New York, NY, USA

Correspondence to: Susanne E. Bauer (susanne.bauer@columbia.edu)

Received: 7 March 2016 – Published in Atmos. Chem. Phys. Discuss.: 11 April 2016
Revised: 29 July 2016 – Accepted: 2 August 2016 – Published: 26 August 2016

Abstract. The spatial distribution of aerosols and their chemical composition dictates whether aerosols have a cooling or a warming effect on the climate system. Hence, properly modeling the three-dimensional distribution of aerosols is a crucial step for coherent climate simulations. Since surface measurement networks only give 2-D data, and most satellites supply integrated column information, it is thus important to integrate aircraft measurements in climate model evaluations. In this study, the vertical distribution of secondary inorganic aerosol (i.e., sulfate, ammonium, and nitrate) is evaluated against a collection of 14 AMS flight campaigns and surface measurements from 2000 to 2010 in the USA and Europe. GISS ModelE2 is used with multiple aerosol microphysics (MATRIX, OMA) and thermodynamic (ISORROPIA II, EQSAM) configurations. Our results show that the MATRIX microphysical scheme improves the model performance for sulfate, but that there is a systematic underestimation of ammonium and nitrate over the USA and Europe in all model configurations. In terms of gaseous precursors, nitric acid concentrations are largely underestimated at the surface while overestimated in the higher levels of the model. Heterogeneous reactions on dust surfaces are an important sink for nitric acid, even high in the troposphere. At high altitudes, nitrate formation is calculated to be ammonia limited. The underestimation of ammonium and nitrate in polluted regions is most likely caused by a too simplified treatment of the NH_3 / NH_4^+ partitioning which affects the HNO_3 / NO_3^- partitioning.

1 Introduction

The impact of aerosols on climate and air quality is a function of their chemical composition, abundance, and spatial distribution. Understanding the vertical profile of aerosols is crucial for radiative forcing calculations (Xu and Penner, 2012), since aerosols interact with radiation directly through absorption and scattering (Bauer and Menon, 2012; Haywood and Boucher, 2000; Stocker et al., 2013), and indirectly via interactions with clouds (Lohmann and Feichter, 2005). Comparisons of model results with organic aerosol aircraft data showed large discrepancies in the free troposphere (Heald et al., 2005, 2011). Sulfate and ammonium nitrate aerosols, although much simpler to model than organics, have not been studied in the vertical in much detail. There is large uncertainty in the magnitude of the forcing induced by sulfate and ammonium nitrate aerosols, with estimates for the preindustrial to present-day direct radiative forcing of sulfate ranging from -0.6 to $-0.2\,\mathrm{W\,m^{-2}}$ while for ammonium nitrate from -0.3 to $-0.03\,\mathrm{W\,m^{-2}}$ (Stocker et al., 2013) under present-day conditions. These forcings are projected to change in the future, driven by trends in precursor emissions. The projected increase in agricultural ammonia emissions, which will result in greater availability of ammonia, contrasted with the projected reductions in NO_x emissions, can lead to an increased relative contribution of ammonium nitrate to the total secondary inorganic aerosol (SIA) abundance, due to the strong projected decrease of sulfate aerosols (Hauglustaine et al., 2014; Hodas et al., 2014). Yet, the effect of these changes on ammonium nitrate concentrations are still a matter of active research: Paulot et al. (2016) showed increases in nitrate load in the free troposphere while surface concentrations decreased, and Pusede et al. (2016) showed changes in tropo-

spheric chemistry in western USA with increased ammonium nitrate production during daytime rather than at night.

Thermodynamically, ammonia tends to neutralize sulfuric acid over the highly volatile nitric acid (Tagaris et al., 2007). The formation of fine-mode nitrate is a function of ammonia, sulfate availability and relative humidity (RH), since its precursor, nitric acid, condenses following thermodynamic equilibrium (Potukuchi and Wexler, 1995a, b). Sulfuric acid and nitric acid also participate in heterogeneous uptake on dust particles, forming coarse sulfate and nitrate, a process that acts as a sink for the gas phase precursors (Bauer and Koch, 2005; Ravishankara, 1997).

In this paper, we evaluate ammonium, nitrate, and sulfate aerosols in the NASA GISS ModelE2 against surface and aircraft observations, extending what Bauer et al. (2007b) did for nitrate aerosol for the year 2000, by using new aerosol configurations that had been implemented in GISS ModelE2 since then, and a substantially extended record of SIA measurements, both from ground stations and various flight campaigns. To assess the model in terms of SIA surface distribution and vertical profiles, we evaluated the performance of three aerosol configurations, described in Sect. 2.1.1, by comparing them against surface data measured over the USA and Europe during 2000–2010, and 14 flight campaigns, as described in Sect. 2.2. We then study the climatology of the model against measurements, both at surface and at higher altitudes (Sects. 3.1–3.3), and explore the model uncertainties with the help of sensitivity experiments (Sect. 3.4).

2 Experimental approach

2.1 Model description

The NASA GISS ModelE2 model (Schmidt et al., 2014) was run with interactive tropospheric (Shindell et al., 2001, 2003) and stratospheric chemistry (Shindell et al., 2006) and coupled with three different aerosol configurations, as described below. A horizontal resolution of 2° in latitude by 2.5° in longitude and a vertical resolution of 40 layers to 0.1 hPa was used. The simulation was nudged using 6-hourly National Centers for Environmental Prediction (NCEP) reanalysis data (Kalnay et al., 1996) for the horizontal wind component. Sea surface temperatures (SSTs) and sea ice cover were prescribed using the Met Office Hadley Center's sea ice and sea surface temperature data set (HadISST1) (Rayner et al., 2003).

The nitrate optical depth of GISS ModelE2 in the CMIP5 archive was found to be problematic, consistent with the findings of Shindell et al. (2013) for a likely too-high nitrate load. The model was using the Henry value of ammonia instead of the effective Henry value, which resulted in large abundances of ammonia, hence ammonium, hence nitrate. In our work, the nitrate scheme had been corrected and nitrate distribution in the column reflects surface sources such as agricultural, industrial, and biomass burning areas.

2.1.1 Aerosols schemes

Two aerosol schemes were used in this study: OMA (One Moment Aerosol) (Koch et al., 2006; Miller et al., 2006) and MATRIX (Multiconfiguration Aerosol TRacker of mIXing state) (Bauer et al., 2008). OMA is a bulk mass scheme with one fine-mode bin of prescribed size for SO_4^{2-}, NH_4^+, and NO_3^-. In OMA, heterogeneous uptake of SO_2 and HNO_3 on dust surfaces is also included, which takes place on the three smallest size bins out of the five size bins used for mineral dust (Bauer et al., 2004, 2007). This was changed after Bauer et al. (2007) where dust was represented in four size classes, and coating on all classes was tracked. MATRIX is a microphysical scheme representing nucleation, condensation, and coagulation. Sulfate is tracked with both number and mass concentrations for 16 populations, which are based on mixing state. MATRIX represents an intermediate level of complexity; only the total mass of nitrate, ammonium, and aerosol water is calculated, and then distributed across populations based on the sulfate abundance in each one of them, assuming internally mixed components. This approach greatly reduces the required number of transported variables.

Due to the focus on SIA in this paper, we will give a brief description of the sulfate and nitrate schemes in our model. The sulfate chemistry module in both schemes, OMA and MATRIX, is based on Koch et al. (1999) and includes prognostic calculation of gas and aqueous phase DMS, MSA, SO_2, and sulfate concentrations. This provides the sulfate mass in the OMA scheme, and provides aqueous sulfate production rates and H_2SO_4 concentrations as input parameters for MATRIX microphysics (Bauer et al., 2008).

To partition between the gas and particle phases the model uses the nonlinear thermodynamics. Both schemes were run coupled to the secondary inorganic aerosol thermodynamics scheme EQSAM (Metzger et al., 2002a, b). MATRIX was also run coupled to ISORROPIA II (Fountoukis and Nenes, 2007), which was only recently introduced into GISS ModelE2. EQSAM is a parameterized thermodynamics scheme that relies on the relationship between activity coefficients and RH to calculate the solute activity and the non-ideal solution properties, while ISORROPIA II calculates the equilibrium constants and solves the thermodynamic equations analytically. Both models use the same input parameters: NH_x (NH_3+NH_4^+), SO_4^{2-}, XNO_3 (HNO_3+NO_3^-), RH and temperature, and interactively calculate the SO_4^{2-}, NH_4^+, NO_3^-, and aerosol H_2O concentrations at equilibrium, as well as the residual NH_3 and HNO_3 in the gas phase.

The thermodynamical equilibrium for Aitken-mode-sized particles, which is important for CCN, might not be properly captured by models (Benduhn et al., 2016). This is not expected to be a problem in this study because Aitken-mode particles are a small fraction of the total aerosol mass. In

addition, for the coarse mode, large uncertainties exist regarding the availability of crustal and coarse-mode material in equilibrium thermodynamic calculations. Our simulations do not take into consideration crustal (e.g., Mg^{2+}, K^{+}, Ca^{2+}) and sea salt (e.g., Na^{+}, Cl^{-}) ions in the thermodynamics, although this option is available in the model.

The model ran in the following three configurations: OMA-EQSAM, MATRIX-EQSAM, and MATRIX-ISORROPIA, and we are comparing model $PM_{2.5}$ (particles with dry diameter smaller than 2.5 µm) with measured $PM_{2.5}$ at surface, and model PM_1 (particles with dry diameter smaller than 1 µm) with measured PM_1 at the vertical, for consistency with the available measurements.

2.1.2 Emissions

This study used the Coupled Model Intercomparison Project phase 5 (CMIP5) historical anthropogenic emissions until 2005 (Lamarque et al., 2010) and the Representative Concentration Pathway 4.5 (RCP4.5) scenario thereafter (van Vuuren et al., 2011). Biomass burning emissions came from the Global Fire Emissions Database (GFED3) inventory (van der Werf et al., 2010). The emissions include seasonal variations for the biomass burning, soil NO_x, and shipping and aircraft sectors (Lamarque et al., 2010), yet lack seasonal variability for all other anthropogenic emissions, including agricultural NH_3 sources. In order to prevent unrealistic ammonium and nitrate aerosol loads during wintertime, the agricultural NH_3 emissions were altered using the local solar zenith angle, in order to produce a more realistic seasonal variability, but kept the total annual emissions the same. This approach is comparable to Adams et al. (1999) and Park (2004) who scaled ammonia emissions from crops and fertilizers according to the number of daylight hours.

2.1.3 Sensitivity runs

NH_3 emissions are controlled by the agricultural sector (Lamarque et al., 2010), both in the USA and Europe, where more than 80 % of NH_3 emissions are agriculture related (van Damme et al., 2015; Paulot et al., 2014). We test how changing agricultural NH_3 emissions affect ammonium nitrate formation under two scenarios: doubled and 5 times higher agricultural NH_3 emissions, using the MATRIX-ISORROPIA aerosol configuration. The results of that sensitivity are presented in Sect. 3.4.

2.2 Observational data sets

2.2.1 Surface measurements

We evaluate our simulations against nitrate and sulfate $PM_{2.5}$ data measured by the Interagency Monitoring of Protected Visual Environments (IMPROVE) network over the continental United States (Malm et al., 1994, 2004), and against ammonia, ammonium, nitric acid, nitrate, SO_2, and sulfate

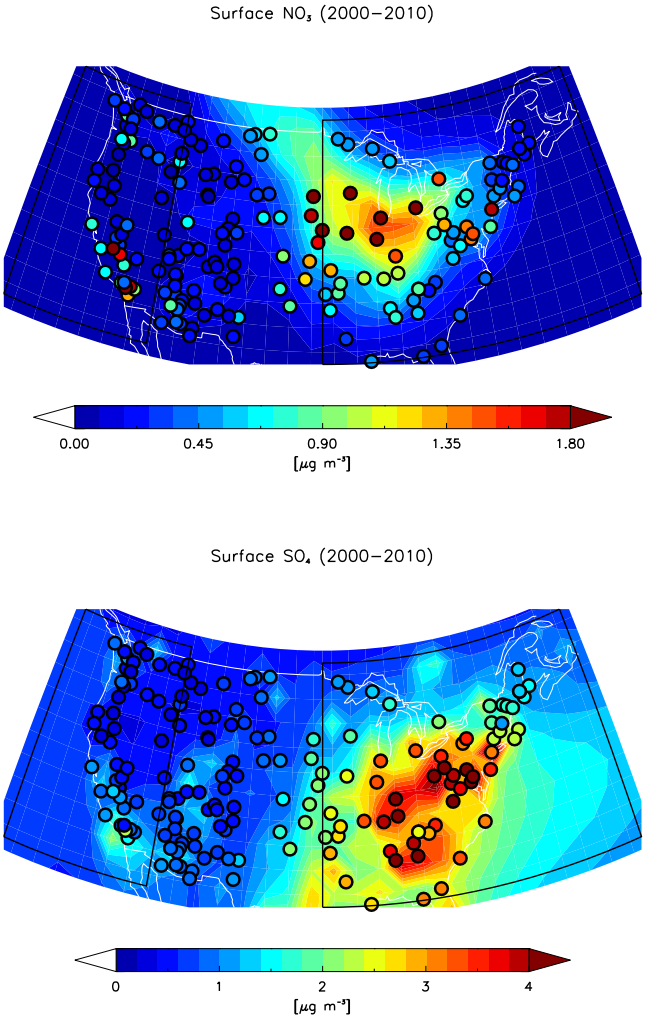

Figure 1. Mean nitrate (upper panel) and sulfate (lower panel) surface concentration (2000–2010) simulated by MATRIX-EQSAM overlaid by measurements from the IMPROVE network. The model data units match the units of the measured data ($\mu g\,m^{-3}$).

measured by the European Monitoring and Evaluation Programme (EMEP), available via the NILU-EBAS database, for the years 2000–2010. From EMEP we use the corrected sulfate for sea salt (XSO_4) (EMEP, 2014, Ch. 3), as it better represents fine sulfate. IMPROVE currently has 212 sites, predominantly rural (Hand et al., 2011, 2012), while EMEP has around 40 sites measuring aerosol composition in Europe, many of which are urban (Tørseth et al., 2012). The data in Europe are reported in $\mu g X\,m^{-3}$ (where X is either sulfur or nitrogen) and in the USA in $\mu g\,m^{-3}$. We decided to keep these units unchanged in the rest of the paper and convert the units of the model to represent those of the measurements, rather than doing the opposite. We compared monthly mean values from all available stations with monthly mean model output. An examination of the mean spatial distribution over the USA (Fig. 1) revealed distinct regimes with different pol-

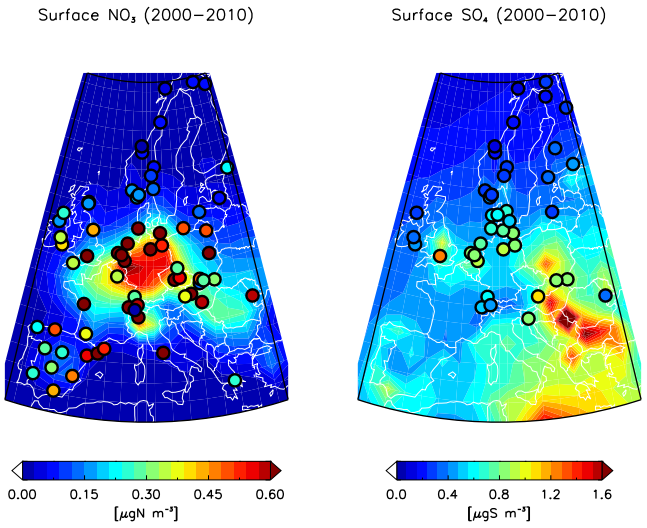

Figure 2. Mean nitrate (left panel) and sulfate (right panel) surface concentration (2000–2010) simulated by MATRIX-EQSAM overlaid by measurements from the EMEP network. The model data units match the units of the measured data ($\mu g X\ m^{-3}$ with X being N for nitrate and S for sulfate).

Table 1. Regional boundaries for data division.

Region	Boundaries
Arctic (ARC)	55–90° N, 60–170° W
Eastern USA (EUSA)	30–50° N, 60–95° W
Western USA (WUSA)	30–50° N, 114–130° W
Europe (ERP)	35–70° N, 10° W–30° E

lution levels, which motivated a regional division of the data into eastern USA (EUSA) and western USA (WUSA). Europe (ERP; Fig. 2) and the Arctic (ARC; data from flight campaigns only) were studied independently (Table 1). The standard deviation, correlation coefficient (R), and normalized mean bias (NMB) between the monthly mean surface values within the studied regions (black frames in Figs. 1 and 2) and the model's monthly mean at the stations locations in each region, were calculated. It is important to note that during the 11-year period the number of measuring sites has varied in each region, and not all stations measured all species.

2.2.2 Flight campaigns

The Aerodyne aerosol mass spectrometer (AMS), which measures chemical composition and size distribution of non-refractory particles (such as ammonium, nitrate, and sulfate) with diameter smaller than 1 µm (Allan et al., 2003; Jimenez et al., 2003), had been part of many flight campaigns in the past decade. Another common method to measure inorganic particle composition is using the particle-into-liquid sampler (PILS), which quantifies the ionic content of particulate matter using ion chromatography (Weber et al., 2001). In this study, we use data from 14 flight campaigns, 2 of which used the PILS instrument for chemical composition measurements, and the rest used the AMS (Table 2). The flights took place in the Northern Hemisphere during short campaign periods, predominantly during spring and summer seasons, between 2001 and 2011. The flight tracks of the campaigns used here are presented in Fig. 3. Data were retrieved using the Tools for Airborne Data interface (https://tad.larc.nasa.gov/), as well as the AMS global database (https://sites.google.com/site/amsglobaldatabase/). For every campaign, a mean regional vertical profile was calculated by averaging the flight data within the model's grid. For short-range campaigns such as ACE, CRISTAL, MILAGRO, TexAQS, and EUCAARI all available data were used, for ITOP the transit flight data were parsed out, and for the rest of the campaigns only data within the regional boundaries we study (black frames in Fig. 3) were used. These boundaries were chosen in accordance with the surface observations.

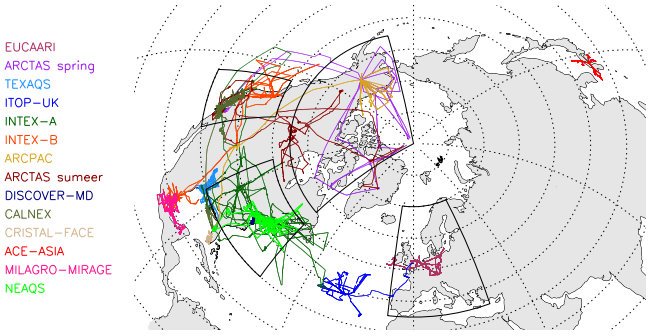

Figure 3. Flight tracks of 14 flight campaigns used in this study (2001–2011).

The campaign-average profile was compared against the monthly mean model output, a not uncommon practice in model–aircraft comparison studies (e.g., Bauer et al., 2007; Emmons et al., 2000; Shindell et al., 2003). The simulations were subsampled by taking into consideration the geographical variability of the flights, but not the submonthly temporal variability, to yield a mean corresponding profile. The 1 standard deviation variability of the campaign data per model level was calculated for the measurements and model simulations, which represents the spatial variability of the concentrations during the whole field campaign for the measurements, and the spatial variability of the monthly mean modeled concentrations for the model. The duration of the field campaigns ranged from 7 to 17 days. In the Results section we picked four representative campaigns that display systematic behavior, one for each region (Fig. 7). The rest of the campaigns can be found in the Appendix A (Figs. A2, A3).

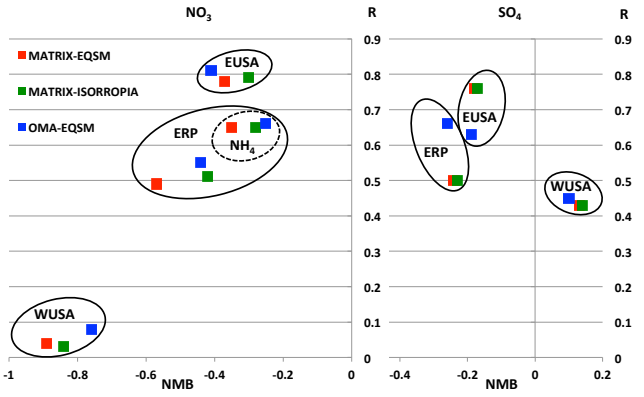

Figure 4. Surface regional statistics (2000–2010). Left panel: nitrate and ammonium (data available only for ERP); right panel: sulfate. The correlation coefficient (R) between the simulation and the measurements is in the y axis, and NMB is in the x axis. MATRIX-EQSAM is in red, MATRIX-ISORROPIA II is in green, and OMA-EQSAM is in blue.

3 Results and discussion

In terms of mean surface concentrations (measured and modeled) in the Western Hemisphere sulfate concentrations are higher than nitrate concentrations. That is not the case in the Eastern Hemisphere, since over western Europe sulfate and nitrate aerosols are comparable in mass (Fig. 2), consistent with Schaap et al. (2004). At the whole atmospheric column (not shown here), sulfate peaks over east ERP and northern Africa due to in-cloud production and transport, while the nitrate column distribution corresponds to the surface distribution, with maxima over the continental hot spots, driven by urban pollution and biomass burning.

3.1 Surface climatology

Surface data show high concentrations of nitrate and sulfate in the industrialized EUSA and ERP and lower concentrations in WUSA, with some urban hot spots (Figs. 1 and 2). We compared the model skill, with respect to measurements, under the three different aerosol configurations in Fig. 4 for nitrate (left) and sulfate (right). The regional clusters observed reflect the fact that performance in terms of R and NMB is controlled by region rather than aerosol scheme. For sulfate, the simulation with no microphysics (OMA, blue) is always biased lower (by 1–4 %) compared to the other two simulations (MATRIX, red and green). This result is due to the microphysical processes included in MATRIX (i.e., nucleation, condensation, and coagulation), which allow for aerosols to spread over the entire size distribution, including the existence of smaller particles (the freshly nucleated ones) which sediment more slowly. Additionally the solubility of sulfate in MATRIX is calculated as a weighted average of the mixed particle component's solubility (SO_4 mixed with

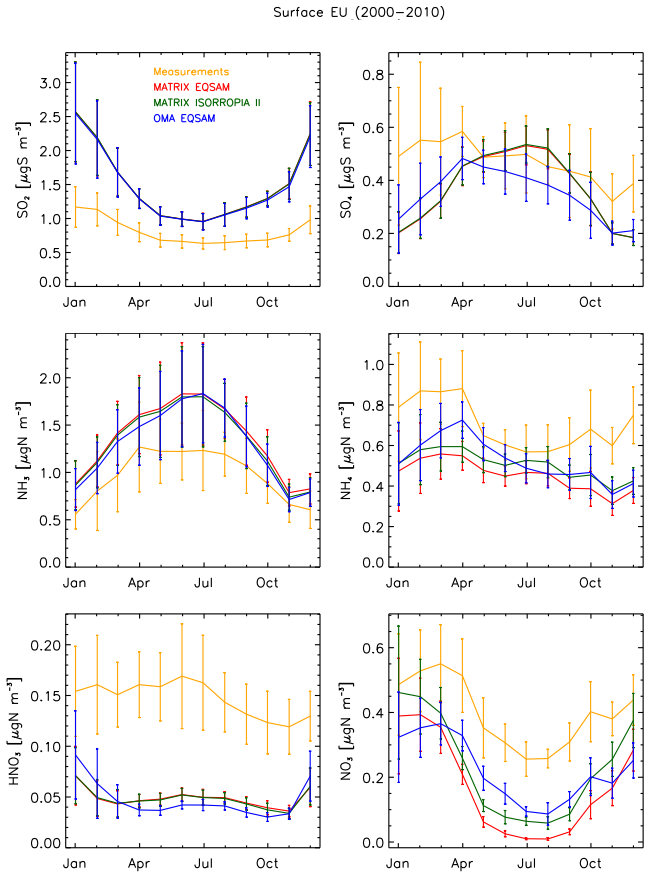

Figure 5. The 2000–2010 mean annual cycle over Europe, error bars represent ±1 standard deviation. Measurements are in orange, MATRIX-EQSAM is in red, MATRIX-ISORROPIA II is in green, and OMA-EQSAM is in blue.

dust, BC, etc.) and is always less than the pure SO_4 solubility in OMA. The differences in both size and solubility lead to a longer lifetime of MATRIX sulfate, thus increasing the aerosol mass. As an indication, the mean lifetime of sulfate in 2005 was 4.2 days in the two MATRIX simulations, against 3.2 days in the OMA simulation. We observe a systematic underestimation of ammonium, nitrate, and sulfate in EUSA and ERP (35 % for nitrate, 30 % for ammonium, 20 % for sulfate). Despite the negative bias, the three aerosol types correlate well with measurements in these regions ($R > 0.5$). This high correlation is due to the fact the simulations successfully capture the aerosol seasonal cycle (discussed in the next section). In the WUSA, the simulations overestimate sulfate by 12 %, and underestimated nitrate by 80 %, while there is no correlation between the model and observations for nitrate. The different behavior across regions reflects the fact that the WUSA is driven by agricultural emissions while in the EUSA industrial and residential emissions dominate. The ability of the model to capture the seasonality is important for model skill and is discussed in the next section.

Table 2. Airborne measurements used in this study.

Campaign (aircraft)	Region (season, year)	Technique and reference	Regime
ACE-Asia (CIPRAS TWIN OTTER)	Japan (spring, 2001)	AMS (Huebert, 2003)	Polluted
CRYSTAL-FACE (CIPRAS TWIN OTTER)	South Florida (summer, 2002)	AMS (Conant et al., 2004)	Polluted
ITOP (BAE-146)	Azores (summer, 2004)	AMS (Fehsenfeld et al., 2006)	Remote
INTEX-A (DC-8, J-31)	Eastern USA (summer, 2004)	CIMS (HNO_3), PILS (SO_4,NH_4,NO_3) (Singh et al., 2006)	Polluted
NEAQS (NOAA-P3)	Eastern USA (summer, 2004)	CIMS (HNO_3), AMS (SO_4, NH_4, NO_3) (Fehsenfeld et al., 2006)	Polluted
INTEX-B (DC-8)	Western USA (spring, 2006)	CIMS (HNO_3), AMS (SO_4,NH_4,NO_3) (Leaitch et al., 2009)	Polluted
MILAGRO (C120)	Mexico (spring, 2006)	AMS (DeCarlo et al., 2008)	Polluted
TexAQS (NOAA-P3)	Texas (fall, 2006)	CIMS (NH_3, HNO_3), AMS (SO_4, NH_4, NO_3) (Parrish et al., 2009)	Polluted
EUCAARI (BAE-146)	NW ERP (spring, 2008)	AMS (Morgan et al., 2010)	Polluted
ARCPAC (NOAA-P3	Arctic (spring, 2008)	CIMS (HNO_3), AMS (SO_4, NH_4, NO_3) (Fisher et al., 2010)	Fire
ARCTAS (DC-8, P-3)	Arctic (spring/summer 2008)	CIMS (HNO_3), AMS (SO_4, NH_4, NO_3) (Jacob et al., 2010)	Fire
CALNEX (NOAA P-3)	West coast (summer, 2010)	CIMS (HNO_3, NH_3), AMS (SO_4, NH_4, NO_3) (Ryerson et al., 2013)	Polluted
DISCOVER-MD (P-3B, UC-12)	Maryland (summer, 2011)	TD-LIF (HNO_3) (Anderson et al., 2014), PILS (SO_4, NH_4, NO_3) (Ziemba et al., 2013)	Polluted

3.2 Surface seasonality

Figure 5 shows that in the ERP there is little variation in the SO_2 seasonality between the three simulations, which is emission-level driven. The modeled surface concentration overestimates measurements by about $0.5\,\mu gS\,m^{-3}$ with an amplified seasonal cycle. Past studies (Dentener et al., 2006; Vestreng et al., 2007) have raised concerns regarding the accuracy of SO_2 emission inventories, which might be part of the explanation of the SO_2 overestimation. Additionally, wintertime chemistry slowdown due to reduced photochemistry increases the SO_2 lifetime, resulting in reduced sulfate formation rates, contributing to the underestimation of sulfate concentration which can be as high as a factor of 2 during winter months. For sulfate, the difference between the simulations is dominated by the aerosol scheme, with the summertime peak being more pronounced in the MATRIX simulations than in the OMA one. As explained in the previous section, MATRIX simulates higher concentrations due to the existence of smaller particles with longer lifetimes compared to OMA. Surface NH_3 (Fig. 5) is overestimated in all three simulations, which might be due to incorrect NH_x partitioning calculated by EQSAM and ISORROPIA II, a hypothesis that is supported by the underestimate of ammonium. Contrary to SO_2 and NH_3, nitric acid is underestimated by the simulations by a factor of 3. This contributes to the underestimation of nitrate in all simulations. The simulated seasonality of nitrate matches that of the measurements, peaking during winter and reaching a minimum during summer Konovalov et al. (2008) identified a slight underestimation of NO_x in emission inventories in southern Europe, which would contribute to underestimations of XNO_3.

IMPROVE has extensive sulfate and nitrate surface data to compare against the model simulations. EMEP provides additional HNO_3 data from nine stations, predominantly around the Great Lakes, which is not enough for a proper regional analysis. Unfortunately, ammonium and gas phase aerosol precursors are not routinely measured via the IMPROVE network. In the eastern USA (Fig. 6) the model simulations exhibit peak sulfate concentrations during summer, with the MATRIX simulations having a stronger seasonality than OMA, which better matches observations. For nitrate, all simulations systematically underestimate measurements during most of the year (by about $0.2\,\mu g\,m^{-3}$), except during winter, where MATRIX slightly overestimates them (less then $0.1\,\mu g\,m^{-3}$). The HNO_3 underestimation by the model, as evident by the limited measurements we obtained in EUSA (Fig. A1), contributes to the nitrate underestimation.

In WUSA, the simulated sulfate and nitrate seasonality (Fig. 6, left panels) is flat compared to the measurements. For sulfate, the measured range is $0.7\,\mu g\,m^{-3}$, while in the MATRIX simulations the range is $0.25\,\mu g\,m^{-3}$ and OMA-EQSAM is $0.15\,\mu g\,m^{-3}$. All simulations underestimate measurements during summer and overestimate them during winter. The measured maximum sulfate concentrations are around summer. This feature is captured by OMA-EQSAM, but the MATRIX simulations calculate spring and fall peaks

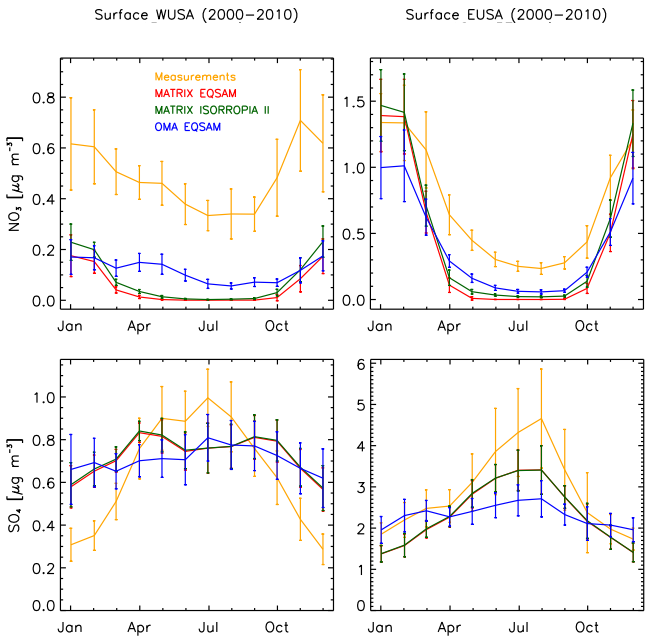

Figure 6. The 2000–2010 mean annual cycle over WUSA (left) and EUSA (right), error bars represent ± 1 standard deviation. Measurements are in orange, MATRIX-EQSAM is in red, MATRIX-ISORROPIA II is in green, and OMA-EQSAM is in blue.

instead. For nitrate, the measurements peak in early winter, a feature that is not captured by the simulations, as modeled nitrate peaks in winter. During the winter OMA-EQSAM and MATRIX EQSAM are similar, probably due to the common thermodynamical scheme, while MATRIX-ISORROPIA II is higher by 0.05 μg m^{-3}. Modeled nitrate is underestimated compared to measurements throughout the year: in the MATRIX simulations it is underestimated by about 0.45 μg m^{-3} (80 % of the measured value), and in OMA-ISORROPIA it is underestimated by about 0.4 μg m^{-3}.

3.3 Vertical profiles

The simulated mean vertical profiles of sulfate, ammonium, nitric acid (when available), and nitrate are evaluated against the mean measured profiles in Fig. 7. The measured and modeled standard deviations (gray shading and dashed lines, respectively), along with the number of days each layer was sampled (black squares), are shown as well. Generally, aerosol concentrations decrease with altitude as they peak near emission sources at the surface. Some of the data used in this study were affected by intense fire plumes (Fisher et al., 2010; Jacob et al., 2010), as can be seen in the ATCPAC (ARC) and ARCTAS spring and summer (ARC) panels (Figs. 7 and A2). Fires act as a source of NO_x, NH_3, and SO_2, increasing the concentration of sulfate, ammonium, and nitrate in the measurements. Fire emissions are included in our simulations, yet these emissions could be underestimated, as Ichoku and Ellison (2014) indicated is the case in many bottom-up emission inventories such as GFED3 (used here), and are also a function of properly resolving the transport. Even if all these factors are accurate in the model, the monthly mean output we use would dilute the signal of a fire event as observed in a flight profile.

Modeled sulfate concentrations are underestimated compared to the measurements (first column in Figs. 7, A2, and A3). The MATRIX simulations that include aerosol microphysics show higher concentrations compared to the bulk scheme. During INTEX-A (EUSA) the MATRIX simulations produced in the boundary layer around 1 μg m^{-3} higher sulfate concentrations compared to OMA. The thermodynamic scheme (EQSAM or ISORROPIA II) makes a minor difference for sulfate, stemming from the simulations' climate feedbacks, with the green and red lines overlaying each other. All these results are consistent with the ones presented earlier for the surface.

In remote environments like the Florida Keys (CRISTAL-FACE, Fig. A3), Azores (ITOP-UK, Fig. A3), and the Arctic (ARCTAS spring and summer, Figs. 7 and A2), ammonium and nitrate concentrations are generally very low, and the models are able to reproduce the aerosol concentrations. However, in campaigns over land such as EUCAARI ERP, EUSA: INTEX-A, NEAQS, DISCOVER-MD, CALNEX WUSA, TexAQS, and Mexico: MILAGRO-MIRAGE, INTEX-B, there is consistent underestimation of both ammonium and nitrate, especially in the boundary layer (Figs. 7, A2 and A3). The sensitivity runs we performed, presented later, explore whether this is due to precursor levels or to the thermodynamic parameterization used.

From the nitric acid profiles (third column in Figs. 7 and A2), it is evident that the model strongly overestimates the measurements in the middle and upper troposphere. HNO_3 overestimation at high altitudes is consistent with Fig. 10 from Shindell et al. (2006). On top of that, the modeled nitric acid shows distinct OMA and MATRIX profiles, which diverge with increasing height, with differences that can become as high as 0.3 ppbv. Though there is not much dust at these altitudes, the inclusion of heterogeneous reactions on dust surfaces in OMA is the main difference in the gas phase chemistry of OMA and MATRIX schemes. The coarse-mode nitrate mass formed by those heterogeneous reactions almost fully accounts for the difference in HNO_3 between the two schemes. However, this loss is insufficient to explain the discrepancy between the model and measurements. We exclude the nitrate that forms on dust (coarse nitrate) from the nitrate profiles, since they are neither in the PM_1 aerosol measurements, nor are they calculated in the MATRIX simulations.

The overestimation of nitric acid does not result in overestimation of nitrate, which is also affected by the availability of both sulfate and ammonia, on top of environmental factors like relative humidity and temperature. Even though nitrate concentrations are low in many locations (below 2 μg m^{-3}), the simulations underestimates it to be below 0.1 μg m^{-3} in EUSA (INTEX-A in Fig. 7, NEAQS, DISCOVER-MD,

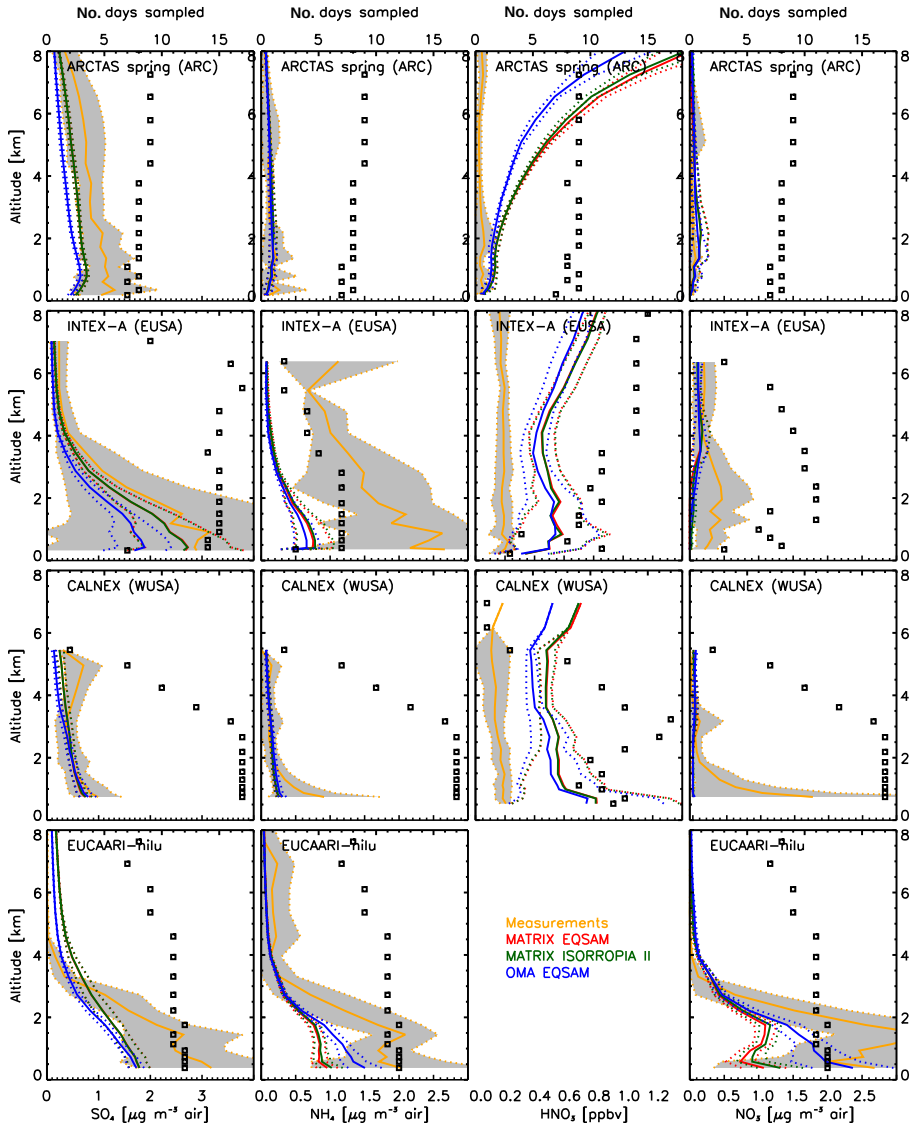

Figure 7. Mean regional concentration profiles from the Arctic (first row), eastern USA (second row), western USA (third row), and Europe (fourth row). First column is SO_4, second is NH_4, third is HNO_3, and fourth is NO_3.

and TexAQS in Fig. A2), WUSA (CALNEX in Fig. 7), Arctic (ARCPAC in Fig. A2), Central America (INTEX-B in Fig. A2, MILAGRO-MIRAGE, and CRISTAL-FACE in Fig. A3), consistent with the spring-summer surface underestimation. Another key point is that there is little difference in the nitrate concentrations simulated by the different aerosol configurations. Differences between the simulations are evident only in the boundary layer in EUCAARI (ERP, Fig. 7) at $\sim 0.8\,\mu g\,m^{-3}$, and ACE-ASIA (Japan, Fig. A3) at $\sim 0.3\,\mu g\,m^{-3}$. In these locations, the difference is not evident on a thermodynamic scheme basis, but rather on a microphysical scheme, with MATRIX-EQSAM and MATRIX-ISORROPIA grouped against OMA-EQSAM. The difference in concentration between the simulations is also evident in the ammonium profiles of these campaigns. In EUCAARI, nitrate and ammonium have higher concentrations in the OMA-EQSAM simulation, while sulfate is consistently larger in the MATRIX ones. In ACE-ASIA, however, both sulfate and ammonium concentrations are higher with OMA-EQSAM, yet nitrate concentrations are higher in the MATRIX simulations. It is evident from these profiles that the simulations with lower sulfate concentrations are also the simulations with higher nitrate concentrations. The role of thermodynamics to the NH_3/NH_4^+ partitioning at different NH_3 levels will be discussed in the next section.

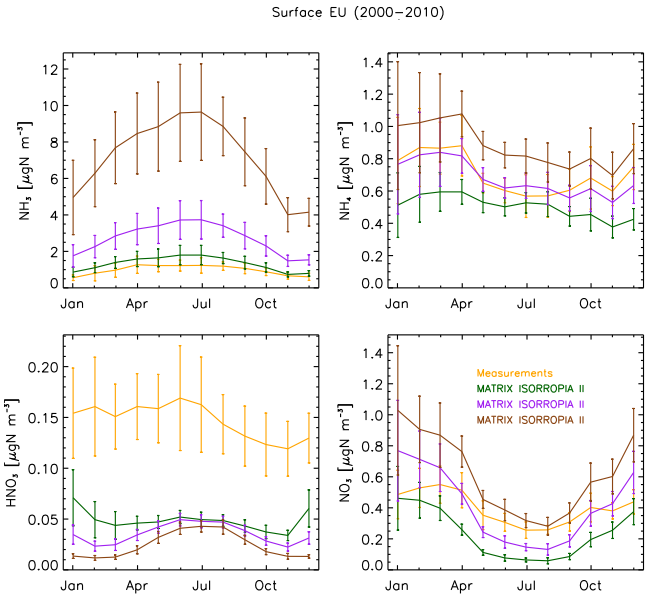

Figure 8. The 2000–2010 mean annual cycle over Europe, error bars represent ± 1 standard deviation. Measurements are in orange, MATRIX-ISORROPIA II with regular emissions is in green, with double agricultural NH_3 emissions in purple, and with 5 times higher agricultural NH_3 emissions in brown.

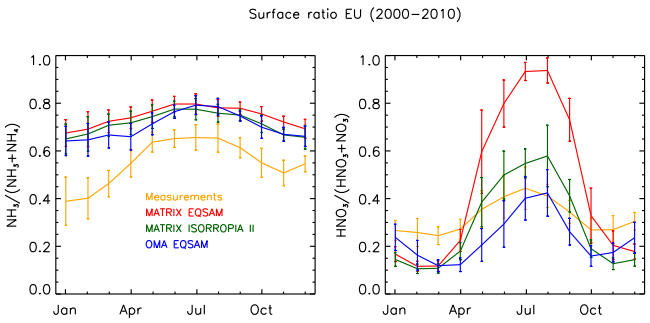

Figure 9. The 2000–2010 mean partitioning ratio annul cycle over Europe, error bars represent ± 1 standard deviation. Measurements are in orange, MATRIX-EQSAM is in red, MATRIX-ISORROPIA II is in green, and OMA-EQSAM is in blue.

3.4 Sensitivity runs

In order to study the interplay between precursor concentrations and thermodynamics, we perturbed the ammonia emissions from agriculture. For these runs, presented in Fig. 8, we use the MATRIX-ISORROPIA scheme with standard NH_3 emission (green line), double agricultural NH_3 emissions (purple line), and 5 times higher agricultural NH_3 emissions (brown line). At the surface, as NH_3 emissions are increased, the ammonium and nitrate underestimation by the model disappears (Fig. 8). However, a comparison with the limited available surface NH_3 measurements reveals that even with the standard NH_3 emissions the model overestimates NH_3 concentrations. This is also evident in TexAQS and CALNEX (WUSA) NH_3 profiles (Fig. A4). Similarly, in the vertical, with increasing NH_3 emissions the nitric acid model overestimation decreases (Fig. A5), as more NH_3 becomes available to react with nitric acid and partition it to the aerosol phase. These results indicate that the NH_3 / NH_4^+ partitioning is not accurately calculated by the model, and that this strongly affects the nitric acid/nitrate partitioning. Further evidence to support our conclusion lies in Fig. 9 and presents the modeled and measured partitioning ratios (NH_3 over total NH_x and HNO_3 over total XNO_3). For NH_x all three simulations are grouped together, while for XNO_3 a distinct difference between the thermodynamic schemes is revealed: MATRIX-EQSAM overestimates the partitioning ratio during the summer, and MATRIX-ISORROPIA II is closer to measurements. From the surface seasonality of the individual species (Fig. 5) it is clear that the divergence in the ratio is driven mainly by nitrate concentrations, as HNO_3 concentrations are the same for MATRIX-EQSAM and MATRIX-ISORROPIA II (red and green curves overlaying each other). The difference between these two simulations in terms of nitrate concentrations is of the order of $0.05\,\mu g\,N\,m^{-3}$ and is most distinct during summer (Fig. 5). Similarly, the difference between the simulations for XNO_3 is greater during summer. Thermodynamically, other than precursor levels, the difference in behavior in summer and the rest of the year is also controlled by temperature and RH.

4 Conclusions

In this work, we used a collection of surface measurements and flight campaigns over the USA and Europe from 2000–2010 to study the regional and vertical distribution of secondary inorganic aerosols and their precursors under different aerosol configurations of the GISS ModelE2. In the USA sulfate aerosol dominate the near-surface SIA composition, but over ERP the nitrate aerosol contribution is comparable in mass.

We compare the behavior of SIA concentrations in high (EUSA, ERP) and low (WUSA) aerosol precursor source regions, as the relative contribution of different sectors generates different chemical regimes. We observe a systematic underestimation of near-surface concentrations in the EUSA and ERP compared to the surface network measurements: 35 % for nitrate, 30 % for ammonium, and 20 % for sulfate. However, despite the negative bias, all three simulations have high correlation coefficients ($R > 0.5$) when compared against surface data. In the WUSA, the results for sulfate and nitrate are different in sign; sulfate is biased high (12 %) with $R = 0.43$, while nitrate is biased low (80 %) with no correlation between the simulations and the measurements ($R < 0.1$). The correlation is also driven by the difficulty of the model to capture the annual cycle of the species.

Microphysics has improved the sulfate simulation, as the MATRIX scheme yields consistently both at the surface and in the vertical, higher sulfate concentrations, due to smaller particles having longer lifetimes compared to OMA, the bulk scheme (4.2 days against 3.2 days). For ammonium nitrate simulations there is an additional level of complexity in the form of accurate thermodynamics, which is sensitive both to the precursors and to environmental parameters such as temperature and humidity. Since we have performed nudged simulations, they do not show big differences in temperature and RH, so the differences between the simulations are expected to be dominated by the thermodynamical scheme and not the underlying meteorological parameters. In terms of precursors, NH_3 is slightly overestimated, as indicated by surface measurements over ERP in Fig. 5 and TexAQS and CALNEX campaigns in Fig. A3. HNO_3 is underestimated at the surface but overestimated at higher levels, and including heterogeneous reactions on dust surfaces decreases the overestimation. A more complex version of MATRIX (that currently does not exist) should include heterogeneous uptake on dust. Overall, aerosol mass is consistently underestimated both at surface and in the boundary layer.

In our sensitivity runs, increasing NH_3 emissions results in NH_3 overestimation; however, it improves our simulated HNO_3 profiles. When more NH_3 is available, it reacts with HNO_3 to form ammonium nitrate, resolving underestimations in the aerosol phase. Hence, the partitioning of NH_x which strongly affects the partitioning of XNO_3 is not accurately simulated in the model. Aan de Brugh et al. (2012) identified an overestimation of gas phase precursors during daytime (equivalent to summer) and an overestimation of aerosol phase species during nighttime (equivalent to winter), and found it to be related to the timescale of vertical mixing against the timescale of thermodynamic equilibrium. This relationship was not analyzed here, since it requires high temporal resolution model output.

An examination of aerosol pH (not presented here) indicated a pH range from 1 to 2 over ERP. This range was recently identified by Weber et al. (2016) as a buffering pH zone where partitioning of ammonium nitrate between the gas and aerosol phases is sensitive. Thus, ions which affect pH might play an important role in nitrate formation. Hence, taking into consideration crustal and sea salt ions could affect our thermodynamics and partitioning in regions where these ions are abundant, as Karydis et al. (2016) demonstrated. However, these are currently tracked as bulk dust and sea salt aerosols in the model. In addition to tracking Na^+, Cl^-, etc. separately, we would need to consider the different timescales of the thermodynamics associated with aerosol size distribution. In the future, we plan to investigate the influence of pH on the results in more detail.

In this paper, we have demonstrated the importance of size-resolved sulfate chemistry. However, currently we treat nitrate as bulk, as it is computationally expensive to add 15 nitrate tracers. Perhaps underestimation of nitrate is not only a matter of thermodynamics but microphysics as well, and that properly resolving the size distribution and considering the chemistry that depends on that would improve our simulations.

5 Data availability

The model data are archived at NASA GISS and can be accessed via ftp after requesting permissions from the authors.

Appendix A

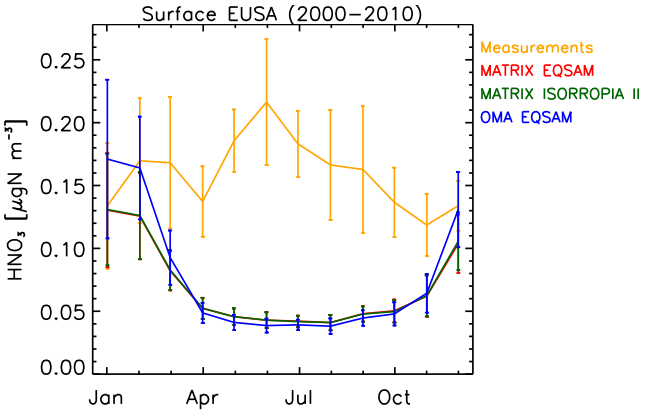

Figure A1. The 2000–2010 HNO_3 mean annual cycle over EUSA (right), error bars represent $\pm$ 1 standard deviation. Measurements are in orange, MATRIX-EQSAM is in red, MATRIX-ISORROPIA II is in green, and OMA-EQSAM is in blue.

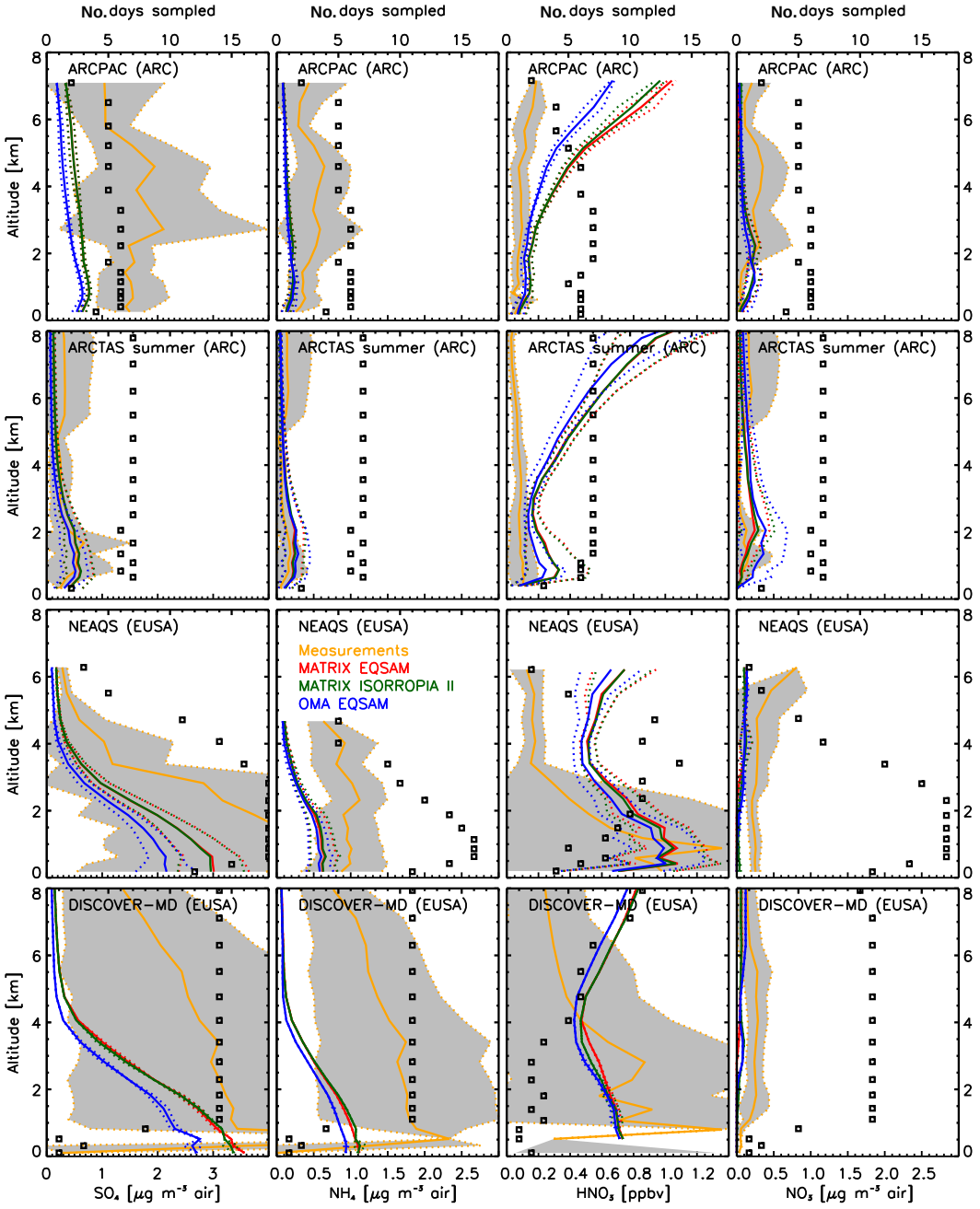
No. days sampled
ARCPAC (ARC)
ARCTAS summer (ARC)
NEAQS (EUSA)
DISCOVER-MD (EUSA)
Measurements
MATRIX EQSAM
MATRIX ISORROPIA II
OMA EQSAM
Altitude [km]
SO4 [μg m-3 air]
NH4 [μg m-3 air]
HNO3 [ppbv]
NO3 [μg m-3 air]

Figure A2.

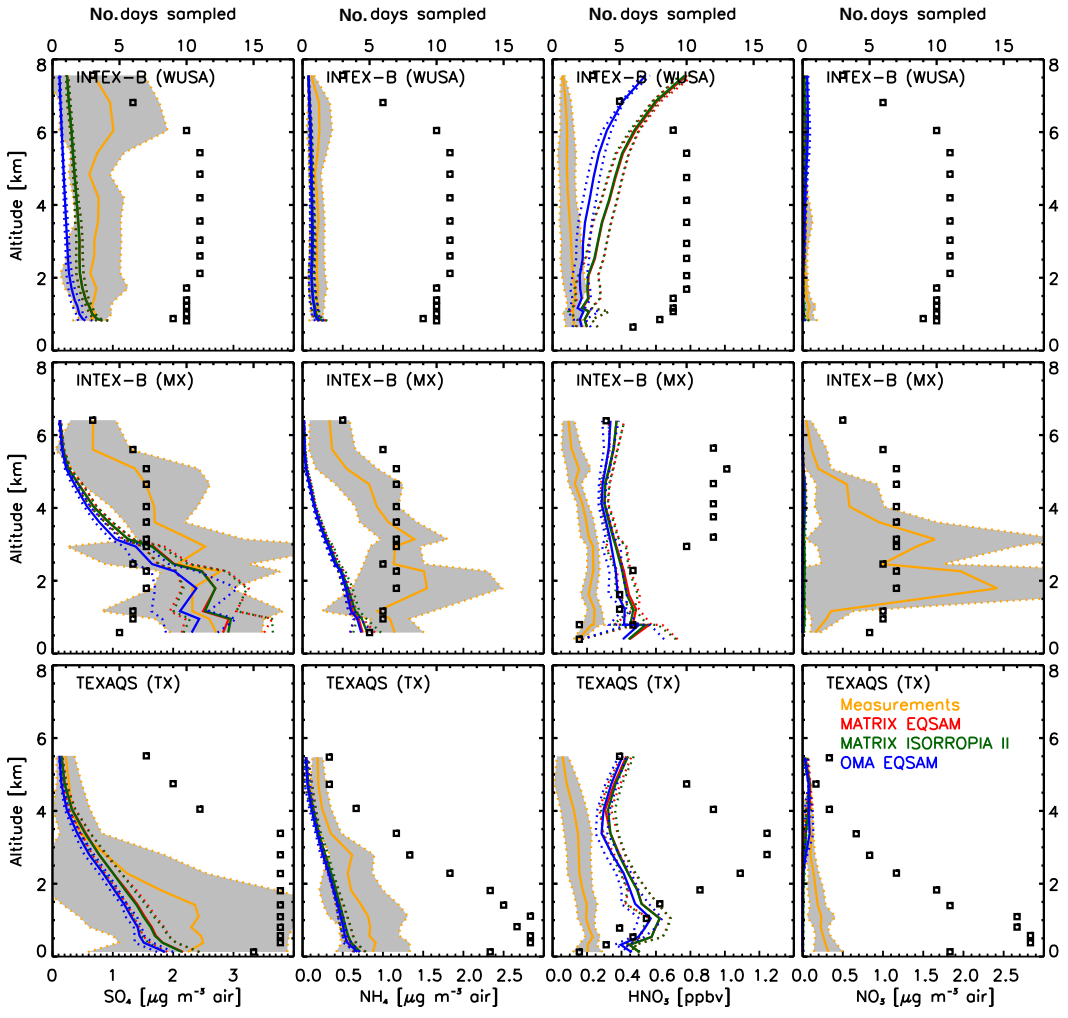

Figure A2. Mean regional concentration profiles. First column is SO_4, second is NH_4, third is HNO_3, and fourth is NO_3. Measurements are in orange, MATRIX-EQSAM is in red, MATRIX-ISORROPIA II is in green, and OMA-EQSAM is in blue.

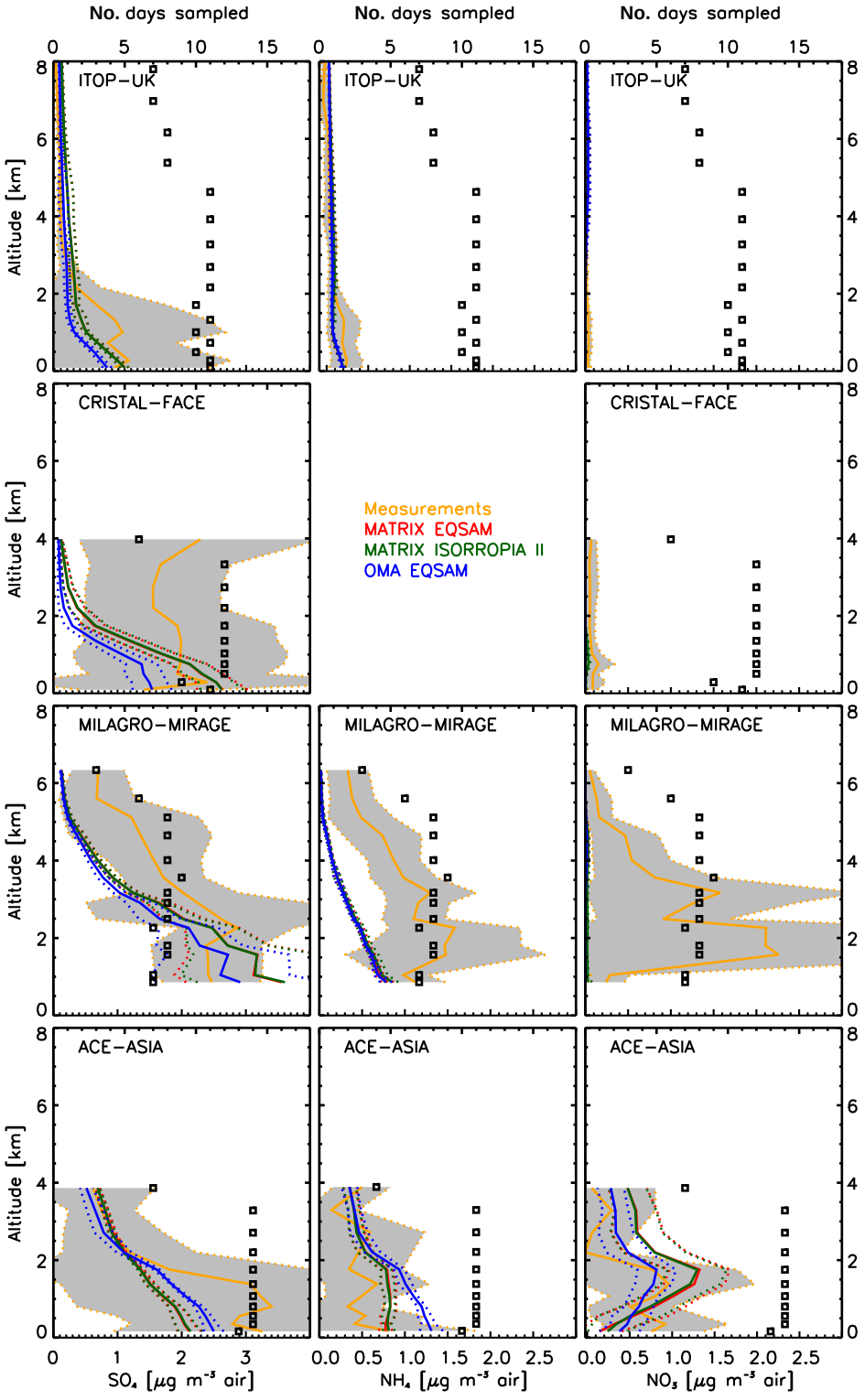

Figure A3. Mean regional concentration profiles. First column is SO_4, second is NH_4, and third is NO_3. Measurements are in orange, MATRIX-EQSAM is in red, MATRIX-ISORROPIA II is in green, and OMA-EQSAM is in blue.

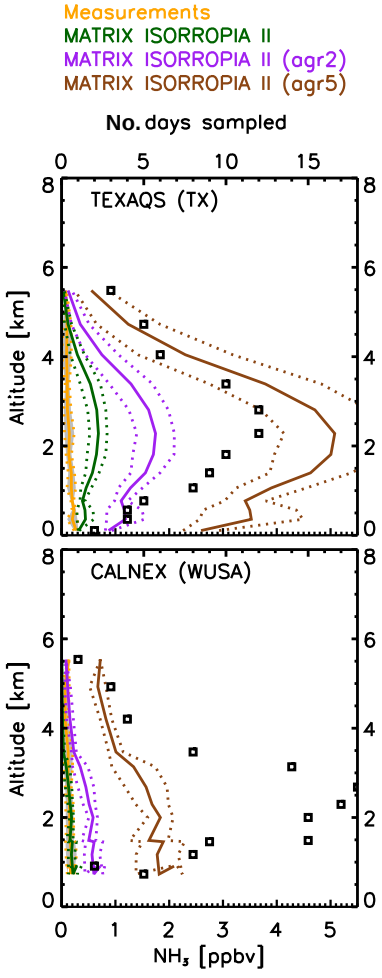

Figure A4. Mean regional NH_3 profiles from the TexAQS (upper panel) and CALNEX (lower panel) campaigns. Measurements are in orange, MATRIX-ISORROPIA II with regular emissions is in green, with double agricultural NH_3 emissions in purple, and with 5 times higher agricultural NH_3 emissions in brown.

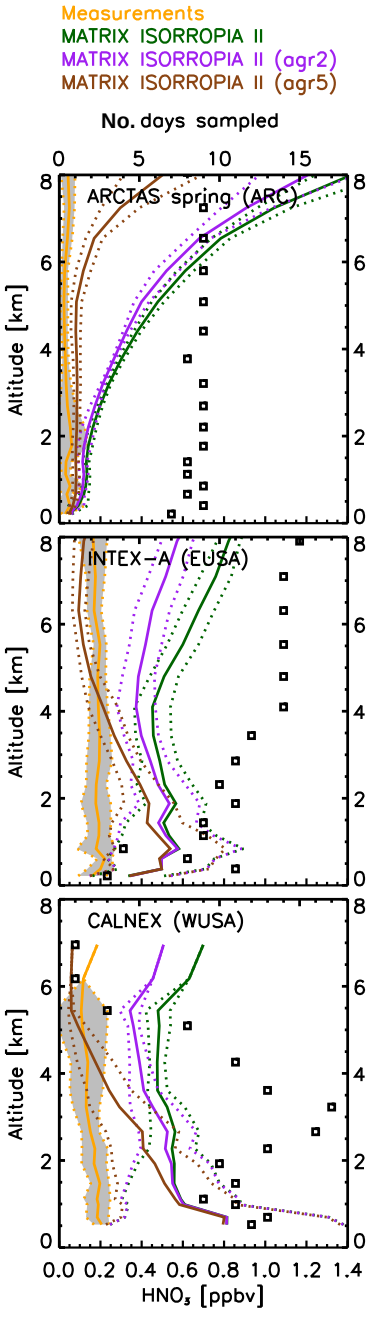

Figure A5. Mean regional HNO_3 profiles from the Arctic, EUSA, and WUSA. Measurements are in orange, MATRIX-ISORROPIA II with regular emissions is in green, with double agricultural NH_3 emissions in purple, and with 5 times higher agricultural NH_3 emissions in brown.

Acknowledgements. Climate modeling at GISS is supported by the NASA Modeling, Analysis, and Prediction program. Resources supporting this work were provided by the NASA High-End Computing (HEC) Program through the NASA Center for Climate Simulation (NCCS) at Goddard Space Flight Center. SEB and KT acknowledge funding from NASA's Atmospheric Composition Modeling and Analysis Program (ACMAP), contract number NNX15AE36G. We acknowledge the IMPROVE monitoring program for providing data. EMEP measurement data were extracted from the EBAS database, which is maintained and further developed by the Norwegian Institute for Air Research (NILU). We acknowledge the Toolsets for Airborne Data (TAD) website: https://tad.larc.nasa.gov, as well as the site https://sites.google.com/site/amsglobaldatabase/ maintained by the Zhang and Jimenez groups.

Edited by: C. Hoyle
Reviewed by: two anonymous referees

References

Aan de Brugh, J. M. J., Henzing, J. S., Schaap, M., Morgan, W. T., van Heerwaarden, C. C., Weijers, E. P., Coe, H., and Krol, M. C.: Modelling the partitioning of ammonium nitrate in the convective boundary layer, Atmos. Chem. Phys., 12, 3005–3023, doi:10.5194/acp-12-3005-2012, 2012.

Adams, P. J., Seinfeld, J. H. and Koch, D. M.: Global concentrations of tropospheric sulfate, nitrate, and ammonium aerosol simulated in a general circulation model, J. Geophys. Res., 104, 13791–13823, 1999.

Allan, J. D., Jimenez, J. L., Williams, P. I., Rami Alfarra, M., Bower, K. N., Jayne, J. T., Coe, H., and Worsnop, D. R.: Correction to "Quantitative sampling using an Aerodyne aerosol mass spectrometer: 1. Techniques of data interpretation and error analysis", J. Geophys. Res., 108, 4283, doi:10.1029/2003JD001607, 2003.

Anderson, D. C., Loughner, C. P., Diskin, G., Weinheimer, A., Canty, T. P., Salawitch, R. J., Worden, H. M., Fried, A., Mikoviny, T., Wisthaler, A. and Dickerson, R. R.: Measured and modeled CO and NOy in DISCOVER-AQ: An evaluation of emissions and chemistry over the eastern US, Atmos. Environ., 96, 78–87, doi:10.1016/j.atmosenv.2014.07.004, 2014.

Bauer, S. E. and Koch, D.: Impact of heterogeneous sulfate formation at mineral dust surfaces on aerosol loads and radiative forcing in the Goddard Institute for Space Studies general circulation model, J. Geophys. Res.-Atmos., 110, 91–105, doi:10.1029/2005JD005870, 2005.

Bauer, S. E. and Menon, S.: Aerosol direct, indirect, semidirect, and surface albedo effects from sector contributions based on the IPCC AR5 emissions for preindustrial and present-day conditions, J. Geophys. Res., 117, 1–15, doi:10.1029/2011JD016816, 2012.

Bauer, S. E., Balkanaki, Y., Schulz, M., and Hauglustaine, D. A.: Global modeling of heterogeneous chemistry on mineral aerosol surfaces: Influence on tropospheric ozone chemistry and comparison to observations, J. Geophys. Res., 109, 1–17, doi:10.1029/2003JD003868, 2004.

Bauer, S. E., Koch, D., Unger, N., Metzger, S. M., Shindell, D. T., and Streets, D. G.: Nitrate aerosols today and in 2030: a global simulation including aerosols and tropospheric ozone, Atmos. Chem. Phys., 7, 5043–5059, doi:10.5194/acp-7-5043-2007, 2007.

Bauer, S. E., Wright, D. L., Koch, D., Lewis, E. R., McGraw, R., Chang, L.-S., Schwartz, S. E., and Ruedy, R.: MATRIX (Multiconfiguration Aerosol TRacker of mIXing state): an aerosol microphysical module for global atmospheric models, Atmos. Chem. Phys., 8, 6003–6035, doi:10.5194/acp-8-6003-2008, 2008.

Benduhn, F., Mann, G. W., Pringle, K. J., Topping, D. O., McFiggans, G., and Carslaw, K. S.: Size-resolved simulations of the aerosol inorganic composition with the new hybrid dissolution solver HyDiS-1.0 – Description, evaluation and first global modelling results, Geosci. Model Dev. Discuss., doi:10.5194/gmd-2015-264, in review, 2016.

Conant, W. C., Vanreken, T. M., Rissman, T. A., Varutbangkul, V., Jonsson, H. H., Nenes, A., Jimenez, J. L., Delia, A. E., Bahreini, R., Roberts, G. C., and Flagan, R. C.: Aerosol–cloud drop concentration closure in warm cumulus, J. Geophys. Res., 109, 1–12, doi:10.1029/2003JD004324, 2004.

DeCarlo, P. F., Dunlea, E. J., Kimmel, J. R., Aiken, A. C., Sueper, D., Crounse, J., Wennberg, P. O., Emmons, L., Shinozuka, Y., Clarke, A., Zhou, J., Tomlinson, J., Collins, D. R., Knapp, D., Weinheimer, A. J., Montzka, D. D., Campos, T., and Jimenez, J. L.: Fast airborne aerosol size and chemistry measurements above Mexico City and Central Mexico during the MILAGRO campaign, Atmos. Chem. Phys., 8, 4027–4048, doi:10.5194/acp-8-4027-2008, 2008.

Dentener, F., Drevet, J., Lamarque, J. F., Bey, I., Eickhout, B., Fiore, A. M., Hauglustaine, D., Horowitz, L. W., Krol, M., Kulshrestha, U. C., Lawrence, M., Galy-Lacaux, C., Rast, S., Shindell, D., Stevenson, D., Van Noije, T., Atherton, C., Bell, N., Bergman, D., Butler, T., Cofala, J., Collins, B., Doherty, R., Ellingsen, K., Galloway, J., Gauss, M., Montanaro, V., Müller, J. F., Pitari, G., Rodriguez, J., Sanderson, M., Solmon, F., Strahan, S., Schultz, M., Sudo, K., Szopa, S., and Wild, O.: Nitrogen and sulfur deposition on regional and global scales: A multimodel evaluation, Global Biogeochem. Cy., 20, GB4003, doi:10.1029/2005GB002672, 2006.

EMEP: EMEP Manual for Sampling and Analysis, EMEP, available at: http://www.nilu.no/projects/ccc/manual/index.html (last access: 30 October 2015), 2014.

Emmons, L. K., Hauglustaine, D. A., Müller, J.-F., Carroll, M. A., Brasseur, G. P., Brunner, D., Staehelin, J., Thouret, V., and Marenco, A.: Data composites of airborne observations of tropospheric ozone and its precursors, J. Geophys. Res., 105, 20497, doi:10.1029/2000JD900232, 2000.

Fehsenfeld, F. C., Ancellet, G., Bates, T. S., Goldstein, A. H., Hardesty, R. M., Honrath, R., Law, K. S., Lewis, A. C., Leaitch, R., McKeen, S., Meagher, J., Parrish, D. D., Pszenny, A. a P., Russell, P. B., Schlager, H., Seinfeld, J., Talbot, R., and Zbinden, R.: International Consortium for Atmospheric Research on Transport and Transformation (ICARTT): North America to Europe – Overview of the 2004 summer field study, J. Geophys. Res.-Atmos., 111, D23S01, doi:10.1029/2006JD007829, 2006.

Fisher, J. A., Jacob, D. J., Purdy, M. T., Kopacz, M., Le Sager, P., Carouge, C., Holmes, C. D., Yantosca, R. M., Batchelor, R. L., Strong, K., Diskin, G. S., Fuelberg, H. E., Holloway, J. S., Hyer, E. J., McMillan, W. W., Warner, J., Streets, D. G., Zhang, Q.,

Wang, Y., and Wu, S.: Source attribution and interannual variability of Arctic pollution in spring constrained by aircraft (ARCTAS, ARCPAC) and satellite (AIRS) observations of carbon monoxide, Atmos. Chem. Phys., 10, 977–996, doi:10.5194/acp-10-977-2010, 2010.

Fountoukis, C. and Nenes, A.: ISORROPIA II: a computationally efficient thermodynamic equilibrium model for K^+–Ca^{2+}–Mg^{2+}–NH_4^+–Na^+–SO_4^{2-}–NO_3^-–Cl^-–H_2O aerosols, Atmos. Chem. Phys., 7, 4639–4659, doi:10.5194/acp-7-4639-2007, 2007.

Hand, J. L., Copeland, S. A., Day, D. E., Dillner, A. M., Indresand, H., Malm, W. C., McDade, C. E., Moore, C. T., Pitchford, M. L., Schichtel, B. A. and Watson, J. G.: Spatial and Seasonal Patterns and Temporal Variability of Haze and its Constituents in the United States Report V., 2011.

Hand, J. L., Schichtel, B. A., Pitchford, M., Malm, W. C., and Frank, N. H.: Seasonal composition of remote and urban fine particulate matter in the United States, J. Geophys. Res., 117, D05209, doi:10.1029/2011JD017122, 2012.

Hauglustaine, D. A., Balkanski, Y., and Schulz, M.: A global model simulation of present and future nitrate aerosols and their direct radiative forcing of climate, Atmos. Chem. Phys., 14, 11031–11063, doi:10.5194/acp-14-11031-2014, 2014.

Haywood, J. and Boucher, O.: Estimates of the Direct and Indirect Radiative Forcing Due to Tropospheric Aerosols: A Review, Rev. Geophys., 38, 513–543, 2000.

Heald, C. L., Jacob, D. J., Park, R. J., Russell, L. M., Huebert, B. J., Seinfeld, J. H., Liao, H., and Weber, R. J.: A large organic aerosol source in the free troposphere missing from current models, Geophys. Res. Lett., 32, 1–4, doi:10.1029/2005GL023831, 2005.

Heald, C. L., Coe, H., Jimenez, J. L., Weber, R. J., Bahreini, R., Middlebrook, A. M., Russell, L. M., Jolleys, M., Fu, T.-M., Allan, J. D., Bower, K. N., Capes, G., Crosier, J., Morgan, W. T., Robinson, N. H., Williams, P. I., Cubison, M. J., DeCarlo, P. F., and Dunlea, E. J.: Exploring the vertical profile of atmospheric organic aerosol: comparing 17 aircraft field campaigns with a global model, Atmos. Chem. Phys., 11, 12673–12696, doi:10.5194/acp-11-12673-2011, 2011.

Hodas, N., Sullivan, A. P., Skog, K., Keutsch, F. N., Collett, J. L., Decesari, S., Facchini, M. C., Carlton, A. G., Laaksonen, A. and Turpin, B. J.: Aerosol liquid water driven by anthropogenic nitrate: implications for lifetimes of water-soluble organic gases and potential for secondary organic aerosol formation., Environ. Sci. Technol., 48, 11127–11136, doi:10.1021/es5025096, 2014.

Huebert, B. J.: An overview of ACE-Asia: Strategies for quantifying the relationships between Asian aerosols and their climatic impacts, J. Geophys. Res., 108, 8633, doi:10.1029/2003JD003550, 2003.

Ichoku, C. and Ellison, L.: Global top-down smoke-aerosol emissions estimation using satellite fire radiative power measurements, Atmos. Chem. Phys., 14, 6643–6667, doi:10.5194/acp-14-6643-2014, 2014.

Jacob, D. J., Crawford, J. H., Maring, H., Clarke, A. D., Dibb, J. E., Emmons, L. K., Ferrare, R. A., Hostetler, C. A., Russell, P. B., Singh, H. B., Thompson, A. M., Shaw, G. E., McCauley, E., Pederson, J. R., and Fisher, J. A.: The Arctic Research of the Composition of the Troposphere from Aircraft and Satellites (ARCTAS) mission: design, execution, and first results, Atmos. Chem. Phys., 10, 5191–5212, doi:10.5194/acp-10-5191-2010, 2010.

Jimenez, J. L., Jayne, J. T., Shi, Q., Kolb, C. E., Worsnop, D. R., Yourshaw, I., Seinfeld, J. H., Flagan, R. C., Zhang, X., Smith, K. A., Morris, J. W., and Davidovits, P.: Ambient aerosol sampling using the Aerodyne Aerosol Mass Spectrometer, J. Geophys. Res., 108, 8425, doi:10.1029/2001jd001213, 2003.

Kalnay, E., Kanamitsu, M., Kistler, R., Collins, W., Deaven, D., Gandin, L., Iredell, M., Saha, S., White, G., Woollen, J., Zhu, Y., Chelliah, M., Ebisuzaki, W., Higgins, W., Janowiak, J., Mo, K. C., Ropelewski, C., Wang, J., Leetmaa, A., Reynolds, R., Jenne, R., and Joseph, D.: The NCEP/NCAR 40-Year Reanalysis Project, B. Am. Meteorol. Soc., 77, 437–471, 1996.

Karydis, V. A., Tsimpidi, A. P., Pozzer, A., Astitha, M., and Lelieveld, J.: Effects of mineral dust on global atmospheric nitrate concentrations, Atmos. Chem. Phys., 16, 1491–1509, doi:10.5194/acp-16-1491-2016, 2016.

Koch, D., Jacob, D., Tegen, I., Rind, D., and Chin, M.: Tropospheric sulfur simulation and sulfate direct radiative forcing in the Goddard Institute for Space Studies general circulation model, J. Geophys. Res., 104, 23799–23822, doi:10.1029/1999JD900248, 1999.

Koch, D., Schmidt, G. A., and Field, C. V.: Sulfur, sea salt, and radionuclide aerosols in GISS ModelE, J. Geophys. Res. Atmos., 111, D06206, doi:10.1029/2004JD005550, 2006.

Konovalov, I. B., Beekmann, M., Burrows, J. P., and Richter, A.: Satellite measurement based estimates of decadal changes in European nitrogen oxides emissions, Atmos. Chem. Phys., 8, 2623–2641, doi:10.5194/acp-8-2623-2008, 2008.

Lamarque, J.-F., Bond, T. C., Eyring, V., Granier, C., Heil, A., Klimont, Z., Lee, D., Liousse, C., Mieville, A., Owen, B., Schultz, M. G., Shindell, D., Smith, S. J., Stehfest, E., Van Aardenne, J., Cooper, O. R., Kainuma, M., Mahowald, N., McConnell, J. R., Naik, V., Riahi, K., and van Vuuren, D. P.: Historical (1850–2000) gridded anthropogenic and biomass burning emissions of reactive gases and aerosols: methodology and application, Atmos. Chem. Phys., 10, 7017–7039, doi:10.5194/acp-10-7017-2010, 2010.

Leaitch, W. R., Macdonald, A. M., Anlauf, K. G., Liu, P. S. K., Toom-Sauntry, D., Li, S.-M., Liggio, J., Hayden, K., Wasey, M. A., Russell, L. M., Takahama, S., Liu, S., van Donkelaar, A., Duck, T., Martin, R. V., Zhang, Q., Sun, Y., McKendry, I., Shantz, N. C., and Cubison, M.: Evidence for Asian dust effects from aerosol plume measurements during INTEX-B 2006 near Whistler, BC, Atmos. Chem. Phys., 9, 3523–3546, doi:10.5194/acp-9-3523-2009, 2009.

Lohmann, U. and Feichter, J.: Global indirect aerosol effects: a review, Atmos. Chem. Phys., 5, 715–737, doi:10.5194/acp-5-715-2005, 2005.

Malm, W. C., Sisler, J. F., Huffman, D., Eldred, R. A., and Cahill, T. A.: Spatial and seasonal trends in particle concentration and optical extinction in the United-States, J. Geophys. Res., 99, 1347–1370, 1994.

Malm, W. C., Schichtel, B. A., Pitchford, M. L., Ashbaugh, L. L., and Eldred, R. A.: Spatial and monthly trends in speciated fine particle concentration in the United States, J. Geophys. Res., 109, D03306, doi:10.1029/2003JD003739, 2004.

Metzger, S., Dentener, F., Krol, M., Jeuken, A., and Lelieveld, J.: Gas/aerosol partitioning 2. Global modeling results, J. Geophys. Res.-Atmos., 107, 1–23, doi:10.1029/2001JD001103, 2002a.

Metzger, S., Dentener, F., Pandis, S. and Lelieveld, J.: Gas/aerosol partitioning: 1. A computationally efficient model, J. Geophys. Res. Atmos., 107, ACH 16–1.ACH 16–24, doi:10.1029/2001JD001102, 2002b.

Miller, R. L., Cakmur, R. V., Perlwitz, J., Geogdzhayev, I. V., Ginoux, P., Koch, D., Kohfeld, K. E., Prigent, C., Ruedy, R., Schmidt, G. A., and Tegen, I.: Mineral dust aerosols in the NASA Goddard Institute for Space Sciences ModelE atmospheric general circulation model, J. Geophys. Res. Atmos., 111, 1–19, doi:10.1029/2005JD005796, 2006.

Morgan, W. T., Allan, J. D., Bower, K. N., Esselborn, M., Harris, B., Henzing, J. S., Highwood, E. J., Kiendler-Scharr, A., McMeeking, G. R., Mensah, A. A., Northway, M. J., Osborne, S., Williams, P. I., Krejci, R., and Coe, H.: Enhancement of the aerosol direct radiative effect by semi-volatile aerosol components: airborne measurements in North-Western Europe, Atmos. Chem. Phys., 10, 8151–8171, doi:10.5194/acp-10-8151-2010, 2010.

Park, R. J.: Natural and transboundary pollution influences on sulfate-nitrate-ammonium aerosols in the United States: Implications for policy, J. Geophys. Res., 109, D15204, doi:10.1029/2003JD004473, 2004.

Parrish, D. D., Allen, D. T., Bates, T. S., Estes, M., Fehsenfeld, F. C., Feingold, G., Ferrare, R., Hardesty, R. M., Meagher, J. F., Nielsen-Gammon, J. W., Pierce, R. B., Ryerson, T. B., Seinfeld, J. H., and Williams, E. J.: Overview of the second texas air quality study (TexAQS II) and the Gulf of Mexico atmospheric composition and climate study (GoMACCS), J. Geophys. Res.-Atmos., 114, 1–28, doi:10.1029/2009JD011842, 2009.

Paulot, F., Jacob, D. J., Pinder, R. W., Bash, J. O., Travis, K., and Henze, D. K.: Ammonia emissions in the United States, European Union, and China derived by high-resolution inversion of ammonium wet deposition data: Interpretation with a new agricultural emissions inventory (MASAGE-NH_3), J. Geophys. Res.-Atmos., 119, 4343–4364, doi:10.1002/2013JD021130, 2014.

Paulot, F., Ginoux, P., Cooke, W. F., Donner, L. J., Fan, S., Lin, M., Mao, J., Naik, V., and Horowitz, L. W.: Sensitivity of nitrate aerosols to ammonia emissions and to nitrate chemistry: implications for present and future nitrate optical depth, Atmos. Chem. Phys., 15, 25739–25788, doi:10.5194/acpd-15-25739-2015, 2016.

Potukuchi, S. and Wexler, A. S.: Identifying solid-aqueous-phase transitions in atmospheric aerosols. II. Acidic solutions, Atmos. Environ., 29, 3357–3364, doi:10.1016/1352-2310(95)00212-H, 1995a.

Potukuchi, S. and Wexler, A. S.: Identifying solid-aqueous-phase transitions in atmospheric aerosols. I. Neutral-acidity solutions, Atmos. Environ., 29, 1663–1676, doi:10.1016/1352-2310(95)00074-9, 1995b.

Pusede, S. E., Duffey, K. C., Shusterman, A. A., Saleh, A., Laughner, J. L., Wooldridge, P. J., Zhang, Q., Parworth, C. L., Kim, H., Capps, S. L., Valin, L. C., Cappa, C. D., Fried, A., Walega, J., Nowak, J. B., Weinheimer, A. J., Hoff, R. M., Berkoff, T. A., Beyersdorf, A. J., Olson, J., Crawford, J. H., and Cohen, R. C.: On the effectiveness of nitrogen oxide reductions as a control over ammonium nitrate aerosol, Atmos. Chem. Phys., 16, 2575–2596, doi:10.5194/acp-16-2575-2016, 2016.

Ravishankara, A. R.: Heterogeneous and Multiphase Chemistry in the Troposphere, Science, 276, 1058–1065, doi:10.1126/science.276.5315.1058, 1997.

Rayner, N. A., Parker, D. E., Horton, E. B., Folland, C. K., Alexander, L. V., Rowell, D. P., Kent, E. C., and Kaplan, A.: Global analyses of sea surface temperature, sea ice, and night marine air temperature since the late nineteenth century, J. Geophys. Res., 108, 4407, doi:10.1029/2002JD002670, 2003.

Ryerson, T. B., Andrews, A. E., Angevine, W. M., Bates, T. S., Brock, C. A., Cairns, B., Cohen, R. C., Cooper, O. R., De Gouw, J. A., Fehsenfeld, F. C., Ferrare, R. A., Fischer, M. L., Flagan, R. C., Goldstein, A. H., Hair, J. W., Hardesty, R. M., Hostetler, C. A., Jimenez, J. L., Langford, A. O., McCauley, E., McKeen, S. A., Molina, L. T., Nenes, A., Oltmans, S. J., Parrish, D. D., Pederson, J. R., Pierce, R. B., Prather, K., Quinn, P. K., Seinfeld, J. H., Senff, C. J., Sorooshian, A., Stutz, J., Surratt, J. D., Trainer, M., Volkamer, R., Williams, E. J., and Wofsy, S. C.: The 2010 California Research at the Nexus of Air Quality and Climate Change (CalNex) field study, J. Geophys. Res. Atmos., 118, 5830–5866, doi:10.1002/jgrd.50331, 2013.

Schaap, M., van Loon, M., ten Brink, H. M., Dentener, F. J., and Builtjes, P. J. H.: Secondary inorganic aerosol simulations for Europe with special attention to nitrate, Atmos. Chem. Phys., 4, 857–874, doi:10.5194/acp-4-857-2004, 2004.

Schmidt, G. A., Kelley, M., Nazarenko, L., Ruedy, R., Russell, G. L., Aleinov, I., Bauer, M., Bauer, S. E., Bhat, M. K., Bleck, R., Canuto, V., Chen, Y., Cheng, Y., Clune, T. L., Genio, A. Del, Fainchtein, R. De, Faluvegi, G., Hansen, J. E., Healy, R. J., Kiang, N. Y., Koch, D., Lacis, A. a, Legrande, A. N., Lerner, J., Lo, K. K., Matthews, E. E., Menon, S., Miller, R. L., Oinas, V., Oloso, A. O., Perlwitz, J. P., Puma, M. J., Putman, W. M., Rind, D., Romanou, A., Sato, M., Shindell, D. T., Sun, S., Syed, R. A., Tausnev, N., Tsigaridis, K., Unger, N., Voulgarakis, A., Yao, M.-S., and Zhang, J.: Configuration and assessment of the GISS ModelE2 contributions to the CMIP5 archive, J. Adv. Model. Earth Syst., 6, 141–184, doi:10.1002/2013MS000265, 2014.

Shindell, D. T., Garenfell, L. J., Rind, D., Grewel, V., and Price, C.: Chemistry-climate interactions in the Goddard Institute for Space Studies general circulation model 1. Tropospheric chemistry model description and evaluation, J. Geophys. Res., 106, 8047–8075, 2001.

Shindell, D. T., Faluvegi, G., and Bell, N.: Preindustrial-to-present-day radiative forcing by tropospheric ozone from improved simulations with the GISS chemistry-climate GCM, Atmos. Chem. Phys., 3, 1675–1702, doi:10.5194/acp-3-1675-2003, 2003.

Shindell, D. T., Faluvegi, G., Unger, N., Aguilar, E., Schmidt, G. A., Koch, D. M., Bauer, S. E., and Miller, R. L.: Simulations of preindustrial, present-day, and 2100 conditions in the NASA GISS composition and climate model G-PUCCINI, Atmos. Chem. Phys., 6, 4427–4459, doi:10.5194/acp-6-4427-2006, 2006.

Shindell, D. T., Lamarque, J.-F., Schulz, M., Flanner, M., Jiao, C., Chin, M., Young, P. J., Lee, Y. H., Rotstayn, L., Mahowald, N., Milly, G., Faluvegi, G., Balkanski, Y., Collins, W. J., Conley, A. J., Dalsoren, S., Easter, R., Ghan, S., Horowitz, L., Liu, X., Myhre, G., Nagashima, T., Naik, V., Rumbold, S. T., Skeie, R., Sudo, K., Szopa, S., Takemura, T., Voulgarakis, A., Yoon, J.-H.,

and Lo, F.: Radiative forcing in the ACCMIP historical and future climate simulations, Atmos. Chem. Phys., 13, 2939–2974, doi:10.5194/acp-13-2939-2013, 2013.

Singh, H. B., Brune, W. H., Crawford, J. H., Jacob, D. J., and Russell, P. B.: Overview of the summer 2004 Intercontinental Chemical Transport Experiment-North America (INTEX-A), J. Geophys. Res. Atmos., 111, D24S01, doi:10.1029/2006JD007905, 2006.

Stocker, T. F., Qin, D., Plattner, G.-K., Tignor, M., Allen, S. K., Boschung, J., Nauels, A., Xia, Y., Bex, V., and Midgley, P. M.: IPCC, 2013: Summary for Policymakers. In: Climate Change 2013: The Physical Science Basis. Contribution of Working Group I to the Fifth Assessment Report of the Intergovernmental Panel on Climate Change, Cambridge University Press, Cambridge, United Kingdom and New York, NY, USA, 2013.

Tagaris, E., Manomaiphiboon, K., Liao, K. J., Leung, L. R., Woo, J. H., He, S., Amar, P., and Russell, A. G.: Impacts of global climate change and emissions on regional ozone and fine particulate matter concentrations over the United States, J. Geophys. Res. Atmos., 112, D14312, doi:10.1029/2006JD008262, 2007.

Tørseth, K., Aas, W., Breivik, K., Fjæraa, A. M., Fiebig, M., Hjellbrekke, A. G., Lund Myhre, C., Solberg, S., and Yttri, K. E.: Introduction to the European Monitoring and Evaluation Programme (EMEP) and observed atmospheric composition change during 1972–2009, Atmos. Chem. Phys., 12, 5447–5481, doi:10.5194/acp-12-5447-2012, 2012.

van Damme, M., Erisman, J. W., Clarisse, L., Dammers, E., Whitburn, S., Clerbaux, C., Dolman, A. J., and Coheur, P.: Worldwide spatiotemporal atmospheric ammonia (NH_3) columns variability revealed by satellite, Geophys. Res. Lett., 42, 8660–8668, doi:10.1002/2015GL065496, 2015.

van der Werf, G. R., Randerson, J. T., Giglio, L., Collatz, G. J., Mu, M., Kasibhatla, P. S., Morton, D. C., DeFries, R. S., Jin, Y., and van Leeuwen, T. T.: Global fire emissions and the contribution of deforestation, savanna, forest, agricultural, and peat fires (1997–2009), Atmos. Chem. Phys., 10, 11707–11735, doi:10.5194/acp-10-11707-2010, 2010.

van Vuuren, D. P., Edmonds, J., Kainuma, M., Riahi, K., Thomson, A., Hibbard, K., Hurtt, G. C., Kram, T., Krey, V., Lamarque, J. F., Masui, T., Meinshausen, M., Nakicenovic, N., Smith, S. J., and Rose, S. K.: The representative concentration pathways: An overview, Climate Change, 109, 5–31, doi:10.1007/s10584-011-0148-z, 2011.

Vestreng, V., Myhre, G., Fagerli, H., Reis, S., and Tarrasón, L.: Twenty-five years of continuous sulphur dioxide emission reduction in Europe, Atmos. Chem. Phys., 7, 3663–3681, doi:10.5194/acp-7-3663-2007, 2007.

Weber, R. J., Orsini, D., Daun, Y., Lee, Y.-N., Klotz, P. J., and Brechtel, F.: A Particle-into-Liquid Collector for Rapid Measurement of Aerosol Bulk Chemical Composition, Aerosol Sci. Tech., 35, 718–727, doi:10.1080/02786820152546761, 2001.

Weber, R. J., Guo, H., Russell, A. G., and Nenes, A.: High aerosol acidity despite declining atmospheric sulfate concentrations over the past 15 years, Nat. Geosci., 9, 282–285, doi:10.1038/NGEO2665, 2016.

Xu, L. and Penner, J. E.: Global simulations of nitrate and ammonium aerosols and their radiative effects, Atmos. Chem. Phys., 12, 9479–9504, doi:10.5194/acp-12-9479-2012, 2012.

Ziemba, L. D., Thornhill, K. L., Ferrare, R., Barrick, J., Beyersdorf, A. J., Chen, G., Crumeyrolle, S. N., Hair, J., Hostetler, C., Hudgins, C., Obland, M., Rogers, R., Scarino, A. J., Winstead, E. L., and Anderson, B. E.: Airborne observations of aerosol extinction by in situ and remote-sensing techniques: Evaluation of particle hygroscopicity, Geophys. Res. Lett., 40, 417–422, doi:10.1029/2012GL054428, 2013.